

Monitoring indoor exposure to combustion-derived particles using plants

Peer-reviewed author version

WITTERS, Katrien; PLUSQUIN, Michelle; ASLAM, Imran; AMELOOT, Marcel; ROEFFAERS, B.J. Maarten; SLENDERS, Eli; VANGRONSVELD, Jaco; NAWROT, Tim & BOVE, Hannelore (2020) Monitoring indoor exposure to combustion-derived particles using plants. In: Environmental Pollution, 266 (Part 1) (Art N° 115261).

DOI: 10.1016/j.envpol.2020.115261

Handle: <http://hdl.handle.net/1942/31712>

Monitoring Indoor Exposure to Combustion-Derived Particles using Plants

Katrien Witters^a, Michelle Plusquin^a, Eli Slenders^{b, 1}, Imran Aslam^c, Marcel Ameloot^b, Maarten B.J. Roeffaers^c, Jaco Vangronsveld^a, Tim S. Nawrot^{a,d}, Hannelore Bové^{a,b,}*

^a Centre for Environmental Sciences, Hasselt University, Agoralaan Building D, 3590 Diepenbeek, Belgium

^b Biomedical Research Institute, Hasselt University, Agoralaan Building C, 3590 Diepenbeek, Belgium

^c Centre for Surface Chemistry and Catalysis, Leuven University, Celestijnenlaan 200f-box 2461, 3001 Leuven, Belgium

^d Department of Public Health and Primary Care, Leuven University, Herestraat 49 box 706, 3000 Leuven, Belgium

¹ Eli Slenders, Molecular Microscopy and Spectroscopy, Istituto Italiano di Tecnologia, Via Enrico Melen 83, 16152 Genua, Italy.

*Corresponding author. Centre for Environmental Sciences, Hasselt University, Agoralaan Building D, 3590 Diepenbeek, Belgium. *Email addresses:* hannelore.bove@uhasselt.be (H. Bové).

Abstract

Indoor plants can be used to monitor atmospheric particulates. Here, we report the label-free detection of combustion-derived particles (CDPs) on plants as a monitoring tool for indoor pollution. First, we measured the indoor CDP deposition on Atlantic ivy leaves (*Hedera hibernica*) using two-photon femtosecond microscopy. Subsequently, to prove its effectiveness for using it as a monitoring tool, ivy plants were placed near five different indoor sources. CDP particle area and number were used as output metrics. CDP values ranged between a median particle area of 0.45×10^2 to $1.35 \times 10^4 \mu\text{m}^2$, and a median particle number of 0.10×10^2 to 1.42×10^3 particles for the indoor sources: control (greenhouse) < milling machine < indoor smokers < wood stove < gas stove < laser printer. Our findings demonstrate that Atlantic ivy, combined with label-free detection, can be effectively used in indoor atmospheric monitoring studies.

Main finding

Two-photon femtosecond microscopy can be used to selectively measure the deposition of combustion-derived particles on indoor plants at different exposure levels.

Keywords

Indoor pollution; Combustion-derived particles; Monitoring; Ivy

1. Introduction

Indoor air quality is an essential determinant of healthy life and well-being, especially since people are spending a large amount of time indoors. Indoor concentrations of air pollutants can significantly increase when important sources of pollutants are present (Bott, 2000; Myers and Maynard, 2005). Particulate matter (PM) is an important indoor pollutant of particular concern with regard to adverse health effects. The EU Directive 2008/50/EC recognized that there is no identifiable threshold for PM exposure below which it would not pose a risk to human health (European Parliament Council of the European Union, 2008), and the 2013 recommendation of the International Agency for Research on Cancer (IARC) identified the PM mixture as a group 1 carcinogen (IARC, 2013). Indoor PM includes both particles of outdoor and indoor origin. Apte and Salvi noted more than 60 sources of indoor air pollution (Apte and Salvi, 2016). The most significant indoor PM sources include fuel used for cooking (Stabile et al., 2014) as well as heating practices (Apte and Salvi, 2016; United States Environmental Protection Agency, 2019), and indoor tobacco smoking (Gerber et al., 2015). Additionally, printers have become common indoor electronic equipment and are high emitters of ultrafine particles (He et al., 2007; Morawska et al., 2019) but also low levels of PM₁₀ and PM_{2.5} are emitted (Tang et al., 2012). These sources generally generate combustion-derived particles (CDPs). CDPs comprise both engineered carbon black (CB) used in and emitted by numerous consumer products such as printer toners, and black carbon (BC) particles that are emitted as an unwanted by-product during the incomplete combustion of fossil fuels, biofuels and biomass (Center for Climate and Energy Solutions, 2010; Climate and Clean Air Coalition, 2016; Long et al., 2013). Those particles are considered one of the most toxic components of PM (Janssen et al., 2011; Krzyzanowski et al., 2005). Recently, our research group has demonstrated that in real-life conditions BC particles, as part of the CDPs,

translocate from the lungs to different organs as shown by their presence in urine (Saenen et al., 2017) and placental tissue (Bové et al., 2019).

Approaches for monitoring air pollution were expensive and required complex equipment, limiting large-scale applicability and accessibility. However, this has changed with the availability of low-cost and easy-to-use air pollution sensors (Snyder et al., 2013). While these detection devices are currently available to monitor the concentrations of gas-phase species or PM in general, no method is readily available for the accurate determination of the CDP fraction in the air pollution mixture. To overcome these challenges, we evaluated the feasibility of the label-free detection of CDPs on indoor plants as a monitoring tool. Already numerous studies have demonstrated the successful use of plant leaves as a monitoring tool of atmospheric PM because of their ability to scavenge and accumulate significant amounts of particulates (Baldacchini et al., 2017; Capozzi et al., 2019; Di Palma et al., 2017; Dzierżanowski et al., 2011; Hofman et al., 2017; Popek et al., 2013; Sæbø et al., 2012). In addition, using plants leaves has been pointed as a rapid, yet reliable approach that enables the collection of site-specific PM. The deposition and accumulation of atmospheric particulates is generally higher with vegetation than with other surfaces such as artificial substrates (Pugh et al., 2012). The accumulation efficiency of leaves varies between plant species, influenced by their phenology (deciduous vs. evergreen) and their micro-morphological characteristics, e.g. wax layer properties, microsurface roughness and presence of trichomes (Popek et al., 2013). For this study, *Hedera hibernica* or Atlantic ivy was selected as test plant because of its known high capacity to scavenge ambient particulates, evergreen foliage, robustness both indoors and outdoors, presence of stomata and trichomes, and resistance to air pollution (Metcalf, 2005; Sternberg et al., 2010). By combining these advantageous features with the label-free detection of the deposited CDPs using two-photon

femtosecond microscopy, as recently developed by Bové et al. (Bové et al., 2016), a very unique monitoring approach is presented. This approach allows the direct visualization of CDPs without the need for sample/particle labeling and/or pretreatment, meaning we are not adding fluorophores and, thus, only fluorescent signals from endogenous compounds are possible. In addition, it allows the specific detection of all carbon-based particles including all CDPs independently of their origin/source. After optimizing and validating the quantification of indoor CDP deposition on the indoor green, our developed monitoring tool was employed to evaluate five different indoor sources producing varying CDP concentrations.

2. Materials and Methods

2.1 Experimental steps for CDP detection

Per location (see section 2.3), four exposed leaves from one plant were selected and three biopsies per leaf were taken on distinct locations between the largest veins, as shown in Figure 1A, using a sterile scalpel and forceps in a clean room with filtered air (Genano 310/OY, Finland, particle filtration cut-off > 0.003 μm) to prevent any external particulate contamination. Each biopsy was placed and taped on a coverslip (Menzel-Gläser, 24'55 mm, 1.5 mm) with the abaxial side facing the glass for inverted imaging (Figure 1B). The CDP deposition on the ivy leaves was identified using a specific and sensitive detection method based on the white light (WL) generation of the particles under two-photon femtosecond illumination, see Figure 1B (Bové et al., 2016). Bové et al. (Bové et al., 2016) observed the WL generation for four different carbon-based particles with diameters ranging from 13 to 500 nm, suggesting that the WL emission under femtosecond near-infrared illumination is a general property of carbon-based particles. Images were collected using a Zeiss LSM 510 (Carl Zeiss, Jena, Germany) confocal laser scanning microscope suitable for non-linear optical imaging, equipped with a two-photon femtosecond pulsed laser (MaiTai

DeepSee, Spectra-Physics, USA; 110 femtoseconds, 80 MHz, 10 mW average laser power on the sample or a power density of $1 \times 10^5 \text{ W/cm}^2$) tuned to a central wavelength of 810 nm. WL from the BC particles was acquired in the non-descanned mode, meaning the emission light is directly reflected on the detector, after spectral separation with a 442 nm dichroic beam splitter and emission filtering employing a 400 – 410 nm band-pass filter. The two-photon excited autofluorescence (TPAF) from the leaves was captured using a short pass dichroic 650 nm beam splitter and a 450 – 650 nm bandpass filter to additionally filter the emission light. Within every biopsy, three spots were chosen randomly and a z-stack throughout the whole leaf (intervals of $6.62 \mu\text{m}$) was made for every spot using a 10x/0.3 (Plan-Neofluar) objective (Figure 1C). Per location, four biological repeats and nine technical repeats were made, resulting in 36 z-stacks, each with a size of $898.20 \times 898.20 \times 6.62 \mu\text{m}^3$ ($1.76 \times 1.76 \times 6.62 \mu\text{m}^3$ voxel size) and recorded with a $3.09 \mu\text{s}$ pixel dwell time.

To quantify the CDPs in the acquired z-stacks, a customized and automated Matlab program (Matlab R2017b (9.3.0.713579), MathWorks, Eindhoven, the Netherlands) was used. The program calculates a maximum projection of the z-stack followed by a peak-find algorithm that detects connected pixels with an intensity above a certain threshold value which was set here 0.03% lower than the highest pixel intensity value of the images (Figure 1D). This threshold resulted in reproducible results without false positive and/or negative values, which was checked using Fiji (ImageJ v2.0, Open source software, <http://fiji.sc/Fiji>). The output metrics ‘particle area’, the total area of the particles in the field of view, and ‘particle number’, the total number of particles in the field of view, were used for further analysis (Figure 1E).

2.2 Optimization and validation experiments of CDP detection

To evaluate the differences in CDP deposition in relation to the leaf topography at the abaxial and adaxial side, the deposited CDP areas of both sides were analyzed after exposure.

The emission fingerprints of the detected CDP particles on the leaves and TPAF from the leaves were recorded using a Zeiss LSM 880 confocal laser scanning microscope suitable for non-linear optical imaging equipped with the same two-photon femtosecond pulsed laser as described for the LSM 510 system. This setup allowed accurate detection of the emission fingerprint of the particles. Gain and laser power were changed to avoid saturation of the emission signal so that the WL signal could be observed over the range from 410 to 650 nm: signals were collected in 9.7 nm bins of a QUASAR thirty-two channel GaASP spectral detector (Carl Zeiss, Jena, Germany). The resulting 1024×1024 lambda image with a pixel size of $0.104 \mu\text{m}$ was detected with a pixel dwell time of $2.05 \mu\text{s}$. The emission fingerprint of commercially available CB nanoparticles (CCB; US Research Nanomaterials, USA) was recorded as a reference using identical settings.

Following femtosecond pulsed laser illumination, the temporal responses of the emitted signals originating from the CDPs on the leaves, from the ivy leaf cells themselves and from reference particles dried on a coverslip were detected using the BiG.2 GaASP detector of the LSM 880 microscope. The detector was coupled with an SPC 830 card (Becker and Hickl, Germany), which was synchronized to the pulse train of the MaiTai DeepSee laser. Recordings of 256×256 images with a pixel size of $0.346 \mu\text{m}$ were acquired using a pixel dwell time of $8.19 \mu\text{s}$. The instrument response function (IRF) was determined by detecting the temporal response of the laser pulse using potassium dihydrogen phosphate crystals. The obtained IRF was used for the analysis of all other temporal measurements for curve fitting. Time-correlated single photon counting measurements were captured using SPCM 9.80 software and analyzed using SPCImage 7.3 software (Becker and Hickl).

In Raman spectra, the carbon fingerprint of the deposited particles was much weaker than and indistinguishable from the autofluorescence of the leaves, the leaves were chemically quenched for 2 h in 0.5% Sudan Black in methanol. Raman measurements were performed on an inverted optical microscope (TiU, Nikon, Japan) equipped with a piezoelectric stage on a home-built optical platform. Continuous-wave laser light from 488 nm Argon Ion laser (Spectra-Physics, USA) with an average power of 10 to 15 mW was reflected by a dichroic mirror (Chroma, ZT488rdc, USA) and focused onto the sample with the objective (60x, Plan Fluor, N.A. 0.85, Nikon, Japan). Raman scattered light from the sample was collected using the same objective and directed to a CCD camera (Newton 920, Andor, UK) equipped with a blazed grating monochromator (IHR-320, Horiba, Japan) with a grating of 1200 g/mm. The Raman signal passed through the 500 nm long-pass filter (Chroma, HQ500LP, USA) after a 100 μ m pinhole for confocal detection. The slit width was set to 2000 μ m. The acquisition time was set to 1 s with averages of 50 acquisitions to increase the signal to noise ratio. The data were analyzed and fitted using OriginPro (version 2018b (9.55), USA) and Fityk (version 0.9.8, open-source software, <https://fityk.nieto.pl/>) (Wojdyr, 2010). The background was corrected for the ivy leaf tissue and reference particles following Cadusch P.J. *et al.* (Cadusch et al., 2013). The Raman spectra of CB nanoparticles were recorded on dry powder as a reference using identical settings.

2.3 Study design indoor sources

To assess our monitoring tool, five indoor sources with varying CDP concentrations and one control were selected: (1) gas stove (Diepenbeek, Belgium), (2) wood stove (Beringen, Belgium), (3) laser printer (Diepenbeek, Belgium), (4) milling machine (Bilzen, Belgium), (5) indoor smokers (Leopoldsburg, Belgium), (6) control (greenhouse of Hasselt University, Diepenbeek, Belgium). Two plants were placed near each source to ensure a sufficient amount of

leaves usable for analysis, *i.e.* fully-developed and undamaged (Supplementary Information (SI), Figure S1). Plants were all placed close to (approximately 1 m) the CDP source and were exposed for 46 days (19/03/2018-03/05/2018). The exposure period was based on the advice of Hofman *et al.* (Hofman et al., 2017, 2014) and Hauke *et al.* (Hauke and Schreiber, 1998) about the minimum and maximum exposure period taking into account leaf senescence as well as the exposure period applied in the study of Gawronska & Bakera (Gawrońska and Bakera, 2015). The plants were all placed on a spot with indirect sunlight at a height of 1.0-1.5 m. Participants were asked to water the soil of the plants every week and to not touch, dust nor move them. They were also requested to avoid cross-contamination, meaning CDP contribution from the other sources under study. For example, active and/or passive smoking was only allowed for the location where they smoked indoors and this was also the case for the use of gas and/or wood stoves. The living room with the wood stove had a volume of approximately 45 m³, and the joinery where the milling machine was located was approximately 625 m³. The locations of all other sources had a volume of approximately 25 m³. In none of the locations air conditioning nor forced ventilation was used. The gas stove was used daily and is located in a half-open kitchen with the exhaust system right above the cooking stove. The wood stove was used once a week for approximately 4 h meaning on average 7 times or 28 h of active burning during the study period. In the joinery, the plants were placed on top of a computer numerically controlled milling machine, which was used daily during working hours. For the location with the indoor smokers, two people smoked each a package of 20 cigarettes per day. The laser printer (Canon iR Advance C5540i) was frequently used, on average 632 pages were printed each working day during the study period.

2.4 Leaf sampling

Atlantic ivy plants (*Hedera hibernica*, ø pot 90 mm, all of the same age) were kept in a greenhouse at Hasselt University under controlled conditions (Diepenbeek, Belgium; 60% air humidity, 15h photoperiod, temperature: day 23°C and night 18°C) prior to use. On the first day of the experiment, the leaves of the plants were carefully rinsed with sterile magnesium sulfate (10 mM, Sigma Aldrich, Belgium) in order to remove as much as possible of the pollution present on the leaves. For each plant, one leaf was removed and taped into a Petri dish with the abaxial side facing up, using sterile forceps (SI, Figure S2). Petri dishes were stored in an airtight box in the dark, at constant temperature and humidity until further analysis, *i.e.* ten days after collection of the leaves at the locations. These control leaves were used to study the variations in the initial CDP loading on each plant, which was found to be insignificant (data not shown).

At the end of the experimental period, four leaves in the middle part of the vertical axis of the plant were removed from one of the two plants, randomly chosen in the case that the leaves of both plants were intact, using sterile forceps and placed in separate Petri dishes. Each leaf was fixed with tape in a Petri dish with the abaxial side facing up, to avoid curling and excessive movement of the leaves, and adherence of particles to the bottom of the Petri dish. Samples were then stored as described previously until further analysis, *i.e.* ten days after the collection .

2.5 Statistical analysis

Data was analyzed with GraphPad Prism (version 5.00 for Windows, GraphPad Software, USA). Images were analyzed using Fiji (ImageJ v2.0, Open source software, <http://fiji.sc/Fiji>).

For each indoor source, the CDP particle area and number were expressed as the median and interquartile range (25th, 75th percentile) obtained from the CDP values of the 36 corresponding z-stacks.

Data were not normally distributed, therefore to compare the CDP particle area and number on the indoor plants of the five different indoor sources, a Kruskal-Wallis rank-sum test was applied followed by pairwise comparisons using the Wilcoxon rank-sum test. Multiple testing was accounted for by using a Bonferroni correction (significance level = 0.003) ensuring a control of the family-wise error rate below 0.05. Robustness was analyzed after removal of extreme values identified by being 1.5 times lower or higher than the first and third quartile respectively.

3. Results and Discussion

3.1 Optimization of the experimental steps for label-free CDP detection

Our previously established method based on the white-light (WL) generation (*i.e.* signal ranging over the whole visible spectrum) of CDPs under two-photon femtosecond pulsed laser illumination for the sensitive and specific detection of CDPs was used to study indoor particulate deposition on ivy leaves (Bové et al., 2016). Besides the WL signals originating from the deposited CDPs, the plant tissue generates two-photon excited autofluorescence (TPAF) under the two-photon illumination, which was detected simultaneously. The latter provides useful information on the leaf surface and thickness for determining the spot locations while avoiding veins and the number of z-stack images throughout the leaf tissue. The CDP particles were analyzed based on two features: (i) the WL signals saturate compared to TPAF allowing thresholding of the CDP particles (Figure 1D) and (ii) the WL emission by the CDPs was only captured in a narrow

emission window (400 - 410 nm) in which interference from other signals is unlikely. As output metrics, both particle number and particle area were defined (Figure 1E). In summary, a flowchart of the experimental steps is shown in Figure 1. Every step in the experiment was designed and monitored to exclude any external contamination.

Figure 2 clearly shows that the CDPs tend to aggregate/agglomerate on the leaf surface instead of being localized individually. This influences the metric particle number, which should be taken into account when interpreting the data. The CDPs taken up by the leaves/plant also aggregate/agglomerate in the veins of the leaves. Therefore, biopsies were taken between the principal veins of the leaves and other large veins were avoided during imaging. Leaves containing spider webs and/or an excessive amount of dust were identified by visually examining the leaves through the ocular of the microscope and excluded from the study to avoid any influence on the results. The heterogeneity of CDP deposition on the leaves was taken into account. From optimization measurements (data not shown), we found that the acquisition of at least 36 z-stacks per indoor source (three spots in three biopsies of four exposed leaves) were necessary to obtain reproducible results.

The particle aggregates/agglomerates on the adaxial and abaxial leaf surfaces were analyzed. At every site, both the particle number and area on the adaxial surface were significantly higher than on the abaxial surface (SI, Figure S3). This may be explained by the distinct morphological traits of both sides of the Atlantic ivy leaves. Atlantic ivy leaves have an undulated topography and their epicuticular wax structures are characterized as platelets. While similar micromorphology and wax structure are observed on both leaf surfaces, a high stomatal density on the abaxial side and absence of stomata on the adaxial side are observed. Also, the abaxial surface contains more trichomes (SI, Figure S4), hair-like structures proven to enhance the

accumulation of ambient particles, than the other side of the leaves (Burkhardt, 2010; Castanheiro et al., 2020; Hofman et al., 2017; Li et al., 2019; Metcalfe, 2005; Muhammad et al., 2019). Due to these differences in morphological traits of both surfaces of the ivy leaves and corresponding dissimilarities in particle deposition, the leaf biopsies were imaged from the abaxial towards the adaxial side.

3.2 Validation experiments of CDP detection

Various validation experiments were conducted to confirm the carbonaceous nature of the identified particles on the Atlantic ivy leaves.

First of all, the characteristic features of the emitted WL produced under two-photon femtosecond pulsed illumination and generated by the identified CDP aggregates on the indoor green were verified. As previously described and checked for specificity and sensitivity by Bové et al., and Saenen et al. (Bové et al., 2016; Saenen et al., 2017): (i) the emission fingerprint should stretch over the whole visible spectrum and (ii) the temporal response should be instantaneous. First, the recorded emission fingerprint of the identified CDPs (Figure 3A) shows that indeed the emission signal ranges over the various wavelengths of the visible spectrum. As a reference, the WL signal of commercially CB particles was measured, which confirms the WL emission profile. On the other hand, the emission fingerprint of the TPAF of the leaf consists of a distinct emission peak. Subsequently, the temporal responses of the identified CDP particles, reference particles and TPAF (Figure 3B) were recorded to be 350, 320 and 1470 ps, respectively. The temporal responses of the reference and CDP particles are instantaneous and non-resolved from the instrument

response function. These results are consistent with previously obtained results and validate the carbonaceous nature of the identified CDP particles (Bové et al., 2016).

Additionally, to confirm the carbonaceous nature of the identified CDPs, Raman spectra from the CDPs on the ivy leaves (Figure 4) and from reference particles (SI, Figure S5) were acquired. Raman spectra of both the CDP and REF particles displayed broad D- and G-peaks typically for carbon-based particles and were located at comparable frequencies (Table S1) (Robertson, 2002).

From the performed validation experiments it can be concluded that the identified CDPs are indeed carbon-based particles and thus the particles of interest. In addition, the proposed technique is specific and sensitive for particles, thereby excluding carbon-containing aromatic compounds. Hence, the developed experimental steps present a unique label-free monitoring tool for the screening of CDPs on indoor leaves.

3.3 Evaluation of the developed monitoring tool for five sources

The second general aim of our study was to evaluate the developed monitoring tool comprising the label-free detection of CDP deposition by testing it on Atlantic ivy leaves following indoor particulate pollution.

The obtained results from the different indoor sources are summarized in Figure 5, Table 1 & 2, and Table S2 & S3. The median CDP particle area (Figure 5A) of the leaves from the control plant (greenhouse) ($0.05 \times 10^3 \mu\text{m}^2$) differed significantly ($p < 0.001$) from all other sources. The highest CDP particle area was found on the leaves collected from the plant located near the laser printer, where a median particle area of $1.35 \times 10^4 \mu\text{m}^2$ was found. The particle area measured near

the laser printer differed significantly from the particle areas measured near the wood stove ($4.10 \times 10^3 \mu\text{m}^2$, $p < 0.05$), indoor smokers ($2.64 \times 10^3 \mu\text{m}^2$, $p < 0.01$) and the milling machine ($1.60 \times 10^3 \mu\text{m}^2$, $p < 0.001$). The median CDP particle area of $7.03 \times 10^3 \mu\text{m}^2$ found in the kitchen with the gas stove differed significantly from the indoor smokers ($p < 0.01$) and the milling machine ($p < 0.001$).

Similar results were found for CDP particle number (Figure 5B). The median CDP particle number detected on the leaves of the control plant (greenhouse) (0.01×10^3 particles) differed significantly ($p < 0.001$) from all other sources. The highest median CDP particle number was found on the leaves from the printer room (1.4×10^3 particles), which differed significantly from the number detected near the milling machine (2.5×10^2 particles, $p < 0.001$), where the lowest number of particles was detected. The median particle CDP particle number found in the kitchen with the gas stove (6.6×10^2 particles) differed significantly from the number detected near the milling machine as well ($p < 0.001$). There were no significant differences found between the other sources (Figure 5B, Table 2 and SI, Table S3).

Robustness analysis was performed removing extreme values, but this did not change the conclusions for particle area (SI, Figure S6A and Table S4) and particle number (SI, Figure S6B and Table S5). In summary, for both particle area and number, the indoor sources can be ranked according to increasing CDP deposition on ivy plants as follows: control (greenhouse) < milling machine < indoor smokers < wood stove < gas stove < laser printer.

Our obtained ranking of the different indoor sources based on the identified CDP deposition on the analyzed indoor plants confirmed our expectations. The median CDP particle area and number were the highest for the laser printer, where the printer was intensively used in

an office setting with limited ventilation. Laser printers indeed have been reported to be high emitters of CDPs including CB, which is an important component of printer toner (He et al., 2007; Mitsubishi Chemical, n.d.). In 2007, He et al. (He et al., 2007), demonstrated that approximately 40% of the laser printers tested, did emit submicrometer particles and 27% of them were high particle emitters. They defined high emitters as printers having a ratio > 10 for particle concentrations measured immediately after the first printed page, compared to the control, i.e. the background office concentrations. We found that the median CDP particle area detected from the printer was 2 times higher than from the gas stove, which was scored as being the second highest source of CDPs in our ranking. Compared to the control, the median particle area detected for the printer was even 300 times higher. For particle number, the median of the printer was 1.2 and 140 times higher than of the gas stove and the control, respectively. Both the gas stove and wood stove include the incomplete combustion of gas and wood, respectively. While higher CDP concentrations are expected from wood burning compared to gas cooking, the slightly higher level in the latter might be due to the fact that the gas cooking stove was used on a daily basis, while the wood stove was only used 7 times for a total of 28 h during the experimental period. In addition, the living room with the wood stove was larger in volume than the kitchen with the gas stove (45 vs. 25 m³), which can explain the ranking as well (SI, Figure S7 and Tables S6 and S7). In the case of indoor smoking, high concentrations of CDPs are expected since cigarette smoke contains high amounts of BC, which rapidly increase over the background with statistically significant difference (Ruprecht et al., 2017). Yet, the lower ranking of this source may be attributed to the large volume and well ventilation on a daily basis of the living room in which the plant was located. The plant near the milling machine captured a low amount of CDPs. Although during wood shaving large quantities of PM are produced (Barbosa et al., 2018), it does not include a combustion process and

almost no CDPs are generated and emitted. Normalizing for the volume of the living room with the wood stove, only changed the ranking with the gas stove (SI, Figure S7 and tables S6 and S7), future leaf monitoring studies should take into account the volume and the ventilation of the room wherein the source is located.

While the ranking of the indoor sources was in line with our expectations, we acknowledge that a limitation of our study is that this ranking is based on only one plant at one location for each CDP source. However, our aim was to demonstrate the effectiveness of our proposed monitoring tool and therefore the ranking is only indicative. A second limitation is that the obtained results for the different indoor sources were not validated using real-time measuring equipment that can sample the indoor concentration of BC aerosols. Examples of such real-time equipment include optical measurements using filter-based absorption photometers, such as Aethalometers (Weingartner et al., 2003), particle soot absorption photometers (Bond et al., 1999), and multi-angle absorption photometers (Petzold et al., 2005). Photometers can provide real-time measurements and are therefore highly desirable for detecting short-term peaks in concentrations and tracking sources. However, this method is not uniquely sensitive to BC and only provides an estimation of its mass (Petzold et al., 2013). The light absorption coefficients determined from these methods are often biased since the scattering and absorption properties of particles on the filter are not the same as in the atmosphere (Watson et al., 2005). The conversion of these aerosol light absorption coefficients into a light-absorbing carbon mass concentration requires precise knowledge of the mass-specific absorption cross section which can vary significantly in time and space. The application of this conversion also assumes that BC is the only light-absorbing particulate species present, but cross-sensitivity to mineral dust and organic carbon compounds can influence the outcome (Petzold et al., 2013; Schwarz et al., 2010; Sharma et al., 2017). In

addition, all filter-based optical methods exhibit a filter loading effect that decreases the photometer sensitivity and obtained data require a lot of post-processing to accurately determine the CDP fraction in polluted air (Backman et al., 2017; Drinovec et al., 2014). To avoid additional bias, it is also recommended to use a new filter strip for each sampling campaign, typically one per day. Thus, although various techniques exist to determine CDP content in the air, there is no standard method that generates a consistent and accurate determination of CDPs in polluted air, one of the most toxic fractions of PM. In this study we suggest the use of ivy leaves, which have already shown to be a reliable bio-indicator for PM, as a monitoring tool for CDPs. The deposition efficiency of atmospheric particulates is generally higher to vegetation than to other surfaces due to the micro-morphological attributes of plant leaves that promote the deposition and accumulation of atmospheric particulates on their surface (Pugh et al., 2012). By combining the advantageous features of ivy plants with the label-free detection of the deposited CDPs, we provide a unique tool that can detect and quantify the CDP fraction in the air pollution mixture in a specific and sensitive manner.

4. Conclusions

Our results demonstrate that two-photon femtosecond microscopy can be used to selectively determine the CDP deposition on indoor plants at different exposure levels. Using plants as a biological monitoring tool does not require sophisticated and high maintenance equipment and is particularly suitable for long-term monitoring over large areas. In addition, the ease of sampling, the absence of any necessary expensive technical equipment, and the possibility of determining spatial and temporal trends make plants a very suitable tool. By combining this novel detection approach with the advantageous characteristics of Atlantic ivy in terms of CDP scavenging and accumulation, a plant-based monitoring approach is presented that can discriminate between

different levels of CDPs related to the different user sources. This study can contribute to providing a solution to the demand to improve air quality monitoring thereby enhancing the ability to study the adverse health effects related to indoor air pollutants.

5. Artwork and Figures

Table 1. The median, 25th, and 75th percentile of the area (μm^2) of the CDPs deposited on the ivy leaves near the different sources.

	25th percentile	Median	75th percentile
Control	0.01x10 ³	0.05x10 ³	0.26x10 ³
Milling machine	0.68x10 ³	1.60x10 ³	3.67x10 ³
Indoor smokers	0.93x10 ³	2.64x10 ³	8.91x10 ³
Wood stove	1.16x10 ³	4.10x10 ³	1.01x10 ⁴
Gas stove	4.92x10 ³	7.03x10 ³	1.27x10 ⁴
Printer	3.14x10 ³	1.35x10 ⁴	2.55x10 ⁴

The number of analyzed z-stacks: control (greenhouse) n=22, all other sources n = 36.

Table 2. The median, 25th, and 75th percentile of the number of CDPs deposited on the ivy leaves near the different sources.

	25th percentile	Median	75th percentile
Control	0.04x10 ²	0.01x10 ³	0.33x10 ²
Milling machine	1.26x10 ²	2.48x10 ²	4.88x10 ²
Indoor smokers	1.82x10 ²	3.74x10 ²	1.04x10 ³
Wood stove	1.37x10 ²	4.30x10 ²	1.20x10 ³
Gas stove	5.21x10 ²	6.59x10 ²	1.13x10 ³
Printer	3.41x10 ²	1.42x10 ³	2.35x10 ³

The number of analyzed z-stacks: control (greenhouse) $n=22$, all other sources $n = 36$.

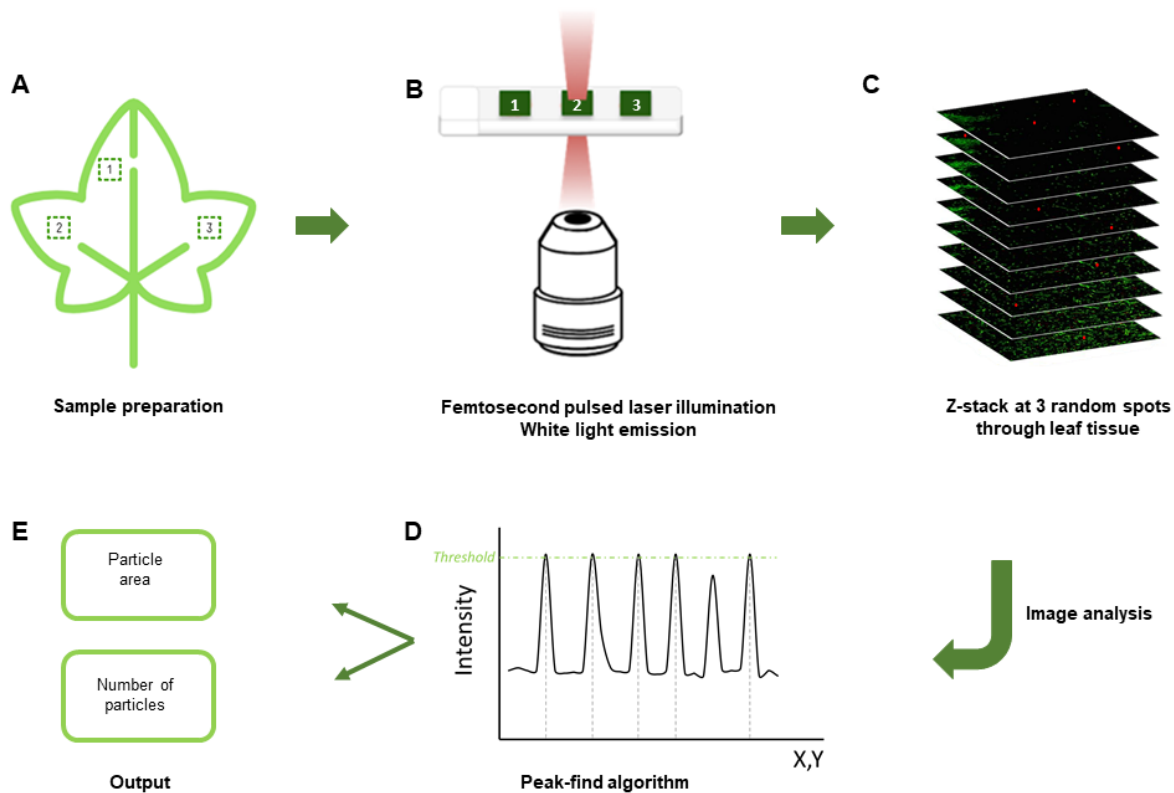


Figure 1. Flowchart of the experimental steps for CDP detection on ivy leaves. (A) From four exposed leaves per indoor source, three standardized biopsies were taken on distinct locations between the largest veins of each leaf. (B) The biopsies were taped on cover slides with the abaxial side facing downwards for inverted imaging. The samples were illuminated using a two-photon femtosecond pulsed laser tuned to a central wavelength of 810 nm (red, 10 mW radiant power at the sample) using a 10x/0.3 objective at room temperature. (C) WL and TPAF signals generated by the CDPs (red) and leaf tissue (green), respectively, were detected (see materials and methods for detailed experimental steps). In total, 36 z-stacks throughout the leaf tissue were taken per

location; three different spots randomly chosen in the three biopsies from four leaves per indoor source. (D) For CDP analysis, a peak-find algorithm counting connected pixels above a threshold value, i.e. 0.03% lower than the highest pixel intensity value of the images, was used. (E) The output metrics were defined as ‘number of particles’ and ‘particle area’. **2-column fitting image, print in color**

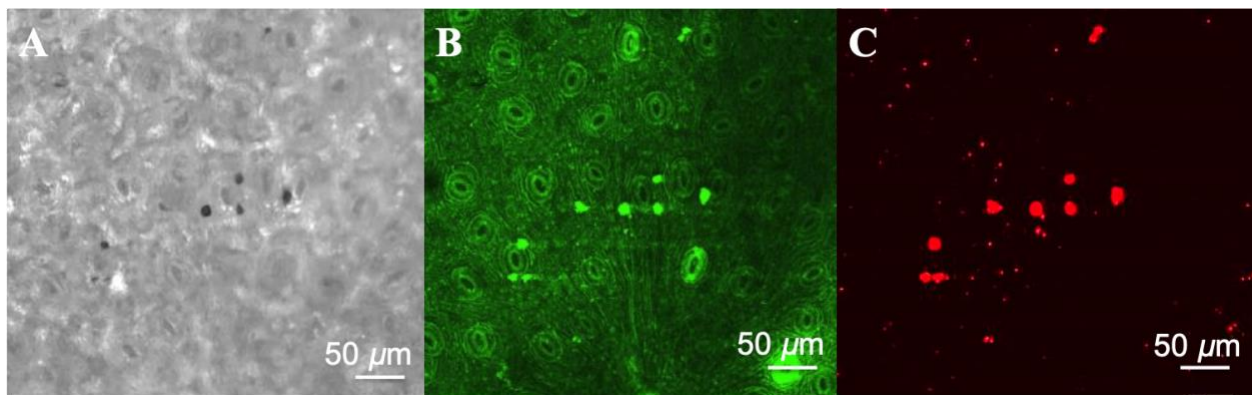


Figure 2. Label-free detection of CDP aggregates deposited on the surface an Atlantic ivy leaf using WL generation under femtosecond pulsed laser illumination (10x/0.3 (Plan-Neofluar) objective, excitation 810 nm, 80 MHz, 10 mW laser power on the sample). (A) Correlative bright field imaging showing the large CDP aggregates as dark spots in the middle of the analyzed abaxial leaf biopsy. (B) Simultaneous detection of the WL signals from the CDP aggregates and the TPAF from the leaf tissue observed at 450-650 nm. (C) Confined detection of the WL signals from the CDP aggregates and single particles observed at 400-410 nm. **2-column fitting image, print in color**

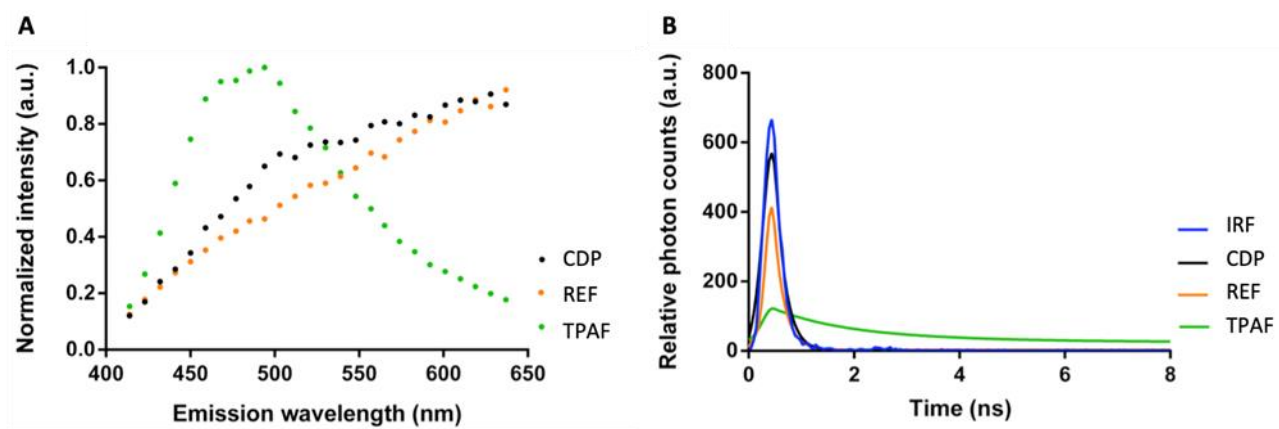


Figure 3. Confirmation of the WL characteristics of the identified CDP particles on the ivy leaves. (A) Emission fingerprint of identified combustion-derived particles (CDP), reference carbon black (REF) particles, and two-photon excited autofluorescence (TPAF) under femtosecond pulsed illumination. (B) Temporal response of CDP and REF particles and TPAF measured by time-correlated single-photon counting. The instrument response function (IRF) of the employed microscopic system is shown in blue. Presented data are from one particle (aggregate/agglomerate) measured in one technical and experimental repeat, and representative for the three experimental repeats performed on three randomly chosen samples. **2-column fitting image, print in color**

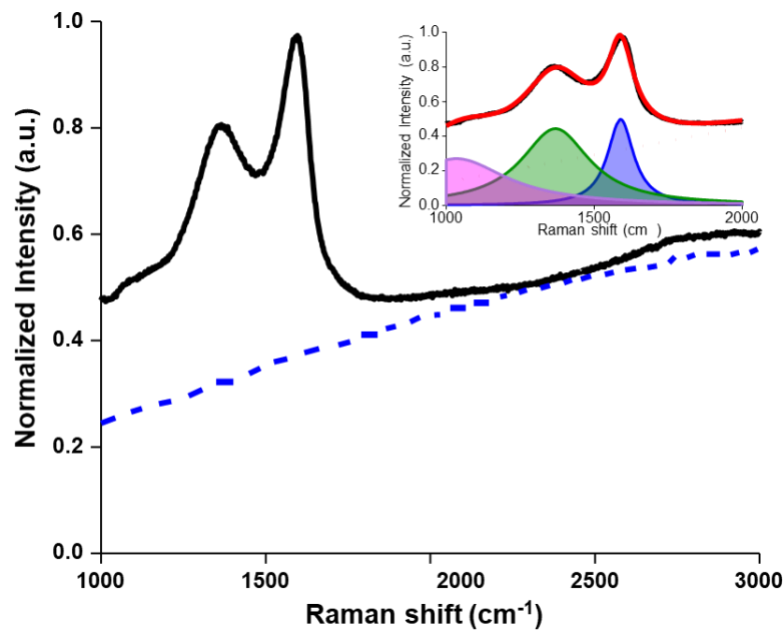


Figure 4. Raman spectra (black solid line) from CDPs on an ivy leaf generating an autofluorescent background (blue dotted line). Inset shows the spectra of the CDPs on the leaves (black line), triple Lorentzian line fit (red), spectral components (purple, green and blue lines) fit results for D-(green) and G-bands (blue), and background correction (red dotted line). Summary of fit results can be found in Table S1. **1.5-column fitting image, print in color**

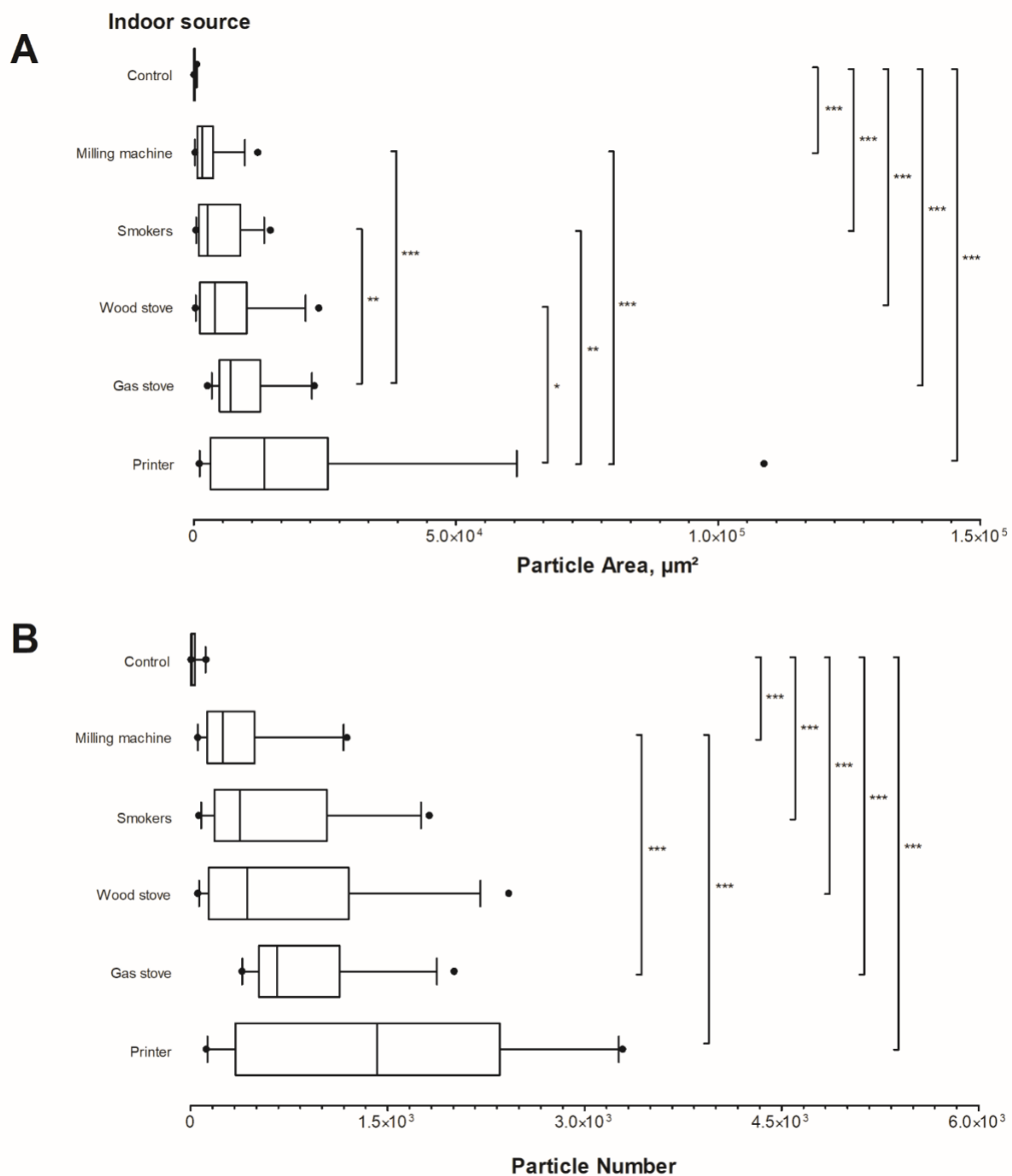


Figure 5. Box plots (median, first and third percentiles, interquartile range, and whiskers indicating 95% of the data) showing (A) the analyzed CDP particle area and (B) the analyzed CDP particle number for the control (greenhouse) (n=22), milling machine (n=36), indoor smokers

458 (n=36), wood stove (n=36), gas stove (n=36), and laser printer (n=36). N indicates the number of
459 analyzed z-stacks per indoor source as a result of four biological and nine technical repeats. Black
460 solid dots represent outliers. *p<0.05, **p<0.01, ***p<0.001. **2-column fitting image, print in**
461 **black-white**

462

463

Acknowledgment

The authors thank Mr. E. Slenders for designing the analysis software in Matlab (Matlab R2017b (9.3.0.713579), MathWorks, Eindhoven, the Netherlands).

Funding Sources

The work was supported by the Flemish Scientific Research Foundation (FWO; fellowship H.B. 12P6819N and project G082317N). The detection equipment was funded by the Interuniversity Attraction Poles Program (P7/05) initiated by the Belgian Science Policy Office and the INCALO project (ERC-PoC).

References

- Apte, K., Salvi, S., 2016. Household air pollution and its effects on health [version 1; peer review: 2 approved]. F1000Research 5. <https://doi.org/10.12688/f1000research.7552.1>
- Backman, J., Schmeisser, L., Virkkula, A., Ogren, J.A., Asmi, E., Starkweather, S., Sharma, S., Eleftheriadis, K., Uttal, T., Jefferson, A., Bergin, M., Makshtas, A., Tunved, P., Fiebig, M., 2017. On Aethalometer measurement uncertainties and an instrument correction factor for the Arctic. Atmos. Meas. Tech. 10, 5039–5062. <https://doi.org/10.5194/amt-10-5039-2017>
- Baldacchini, C., Castanheiro, A., Maghakyan, N., Sgrigna, G., Verhelst, J., Alonso, R., Amorim, J.H., Bellan, P., Bojović, D.Đ., Breuste, J., Bühler, O., Cântar, I.C., Cariñanos, P., Carriero, G., Churkina, G., Dinca, L., Esposito, R., Gawroński, S.W., Kern, M., Le Thiec, D., Moretti, M., Ningal, T., Rantzoudi, E.C., Sinjur, I., Stojanova, B., Aničić Urošević, M., Velikova, V., Živojinović, I., Sahakyan, L., Calfapietra, C., Samson, R., 2017. How Does the Amount and Composition of PM Deposited on *Platanus acerifolia* Leaves Change Across Different Cities in Europe? Environ. Sci. Technol. 51, 1147–1156. <https://doi.org/10.1021/acs.est.6b04052>

486 Barbosa, R.P., Fiedler, N.C., Silva, J.R.M., Souza, A.P. de, Minette, L.J., Oliveira, M.P., 2018.
 487 Concentration and size of airborne particulates in woodworking shops. *Rev. Árvore* 42.
 488 <https://doi.org/10.1590/1806-90882018000100009>
 489 Bond, T.C., Anderson, T.L., Campbell, D., 1999. Calibration and Intercomparison of Filter-Based
 490 Measurements of Visible Light Absorption by Aerosols. *Aerosol Sci. Technol.* 30, 582–600.
 491 <https://doi.org/10.1080/027868299304435>
 492 Bott, R., 2000. The right to healthy indoor air, WHO meeting. Bilthoven, The Netherlands.
 493 <https://doi.org/10.1007/s13398-014-0173-7.2>
 494 Bové, H., Bongaerts, E., Slenders, E., Bijmens, E.M., Saenen, N.D., Gyselaers, W., Van Eyken, P.,
 495 Plusquin, M., Roeffaers, M.B.J., Ameloot, M., Nawrot, T.S., 2019. Ambient black carbon
 496 particles reach the fetal side of human placenta. *Nat. Commun.* 10.
 497 <https://doi.org/10.1038/s41467-019-11654-3>
 498 Bové, H., Steuwe, C., Fron, E., Slenders, E., D’Haen, J., Fujita, Y., Uji-i, H., vandeVen, M.,
 499 Roeffaers, M., Ameloot, M., 2016. Biocompatible Label-Free Detection of Carbon Black
 500 Particles by Femtosecond Pulsed Laser Microscopy. *Nano Lett.* 16, 3173–3178.
 501 <https://doi.org/10.1021/acs.nanolett.6b00502>
 502 Burkhardt, J., 2010. Hygroscopic particles on leaves: nutrients or desiccants? *Ecol. Monogr.* 80,
 503 369–399. <https://doi.org/10.1890/09-1988.1>
 504 Cadusch, P.J., Hlaing, M.M., Wade, S.A., McArthur, S.L., Stoddart, P.R., 2013. Improved
 505 Methods for Fluorescence Background Subtraction from Raman Spectra. *J. Raman Spectrosc.*
 506 44. <https://doi.org/10.1002/jrs.4371>
 507 Capozzi, F., Di Palma, A., Adamo, P., Sorrentino, M.C., Giordano, S., Spagnuolo, V., 2019. Indoor
 508 vs. outdoor airborne element array: A novel approach using moss bags to explore possible

509 pollution sources. Environ. Pollut. 249, 566–572.
 510 <https://doi.org/10.1016/j.envpol.2019.03.012>
 511 Castanheiro, A., Hofman, J., Nuyts, G., Joosen, S., Spassov, S., Blust, R., Lenaerts, S., De Wael,
 512 K., Samson, R., 2020. Leaf accumulation of atmospheric dust: Biomagnetic, morphological
 513 and elemental evaluation using SEM, ED-XRF and HR-ICP-MS. Atmos. Environ. 221,
 514 117082. <https://doi.org/10.1016/j.atmosenv.2019.117082>
 515 Center for Climate and Energy Solutions, 2010. What is black carbon? Factsheet. URL
 516 <https://www.c2es.org/site/assets/uploads/2010/04/what-is-black-carbon.pdf> (accessed
 517 8.16.18).
 518 Climate and Clean Air Coalition, 2016. Black carbon | Climate & Clean Air Coalition. Clim.
 519 Clean Air Coalit. URL <http://www.ccacoalition.org/ru/slcp/black-carbon>
 520 Di Palma, A., Capozzi, F., Spagnuolo, V., Giordano, S., Adamo, P., 2017. Atmospheric particulate
 521 matter intercepted by moss-bags: Relations to moss trace element uptake and land use.
 522 Chemosphere 176, 361–368. <https://doi.org/10.1016/j.chemosphere.2017.02.120>
 523 Drinovec, L., Močnik, G., Zotter, P., Prévôt, A.S.H., Ruckstuhl, C., Coz, E., Rupakheti, M., Sciare,
 524 J., Müller, T., Wiedensohler, A., Hansen, A.D.A., 2014. The “dual-spot” Aethalometer: an
 525 improved measurement of aerosol black carbon with real-time loading compensation. Atmos.
 526 Meas. Tech. Discuss. 7, 10179–10220. <https://doi.org/10.5194/amtd-7-10179-2014>
 527 Dzierżanowski, K., Popek, R., Gawrońska, H., Sæbø, A., Gawroński, S.W., 2011. Deposition of
 528 Particulate Matter of Different Size Fractions on Leaf Surfaces and in Waxes of Urban Forest
 529 Species. Int. J. Phytoremediation 13, 1037–1046.
 530 <https://doi.org/10.1080/15226514.2011.552929>
 531 European Parliament Council of the European Union, 2008. Directive 2008/50/EC of the European

parliament and of the council of 21 May 2008 on ambient air quality and cleaner air for Europe.

Gawrońska, H., Bakera, B., 2015. Phytoremediation of particulate matter from indoor air by *Chlorophytum comosum* L. plants. *Air Qual. Atmos. Heal.* 8, 265–272. <https://doi.org/10.1007/s11869-014-0285-4>

Gerber, A., Hofen-Hohloch, A. V., Schulze, J., Groneberg, D.A., 2015. Tobacco smoke particles and indoor air quality (ToPIQ-II) - A modified study protocol and first results. *J. Occup. Med. Toxicol.* 10. <https://doi.org/10.1186/s12995-015-0047-8>

Hauke, V., Schreiber, L., 1998. Ontogenetic and seasonal development of wax composition and cuticular transpiration of ivy (*Hedera helix* L.) sun and shade leaves. *Planta* 207, 67–75. <https://doi.org/10.1007/s004250050456>

He, C., Morawska, L., Taplin, L., 2007. Particle emission characteristics of office printers. *Environ. Sci. Technol.* 41, 6039–6045. <https://doi.org/10.1021/es063049z>

Hofman, J., Maher, B.A., Muxworthy, A.R., Wuyts, K., Castanheiro, A., Samson, R., 2017. Biomagnetic Monitoring of Atmospheric Pollution: A Review of Magnetic Signatures from Biological Sensors. <https://doi.org/10.1021/acs.est.7b00832>

Hofman, J., Wuyts, K., Van Wittenberghe, S., Samson, R., 2014. On the temporal variation of leaf magnetic parameters: Seasonal accumulation of leaf-deposited and leaf-encapsulated particles of a roadside tree crown. *Sci. Total Environ.* 493, 766–772. <https://doi.org/10.1016/j.scitotenv.2014.06.074>

IARC, 2013. Outdoor air pollution, IARC monographs on the evaluation of carcinogenic risks to humans., Volume 109. ed.

Janssen, N.A.H., Hoek, G., Simic-Lawson, M., Fischer, P., van Bree, L., Brink, H. Ten, Keuken,

555 M., Atkinson, R.W., Ross Anderson, H., Brunekreef, B., Cassee, F.R., 2011. Black carbon as
 556 an additional indicator of the adverse health effects of airborne particles compared with pm10
 557 and pm2.5. *Environ. Health Perspect.* <https://doi.org/10.1289/ehp.1003369>
 558 Krzyzanowski, M., Kuna-Dibbert, B., Schneider, J., 2005. Health effects of transport-related air
 559 pollution.
 560 Li, Y., Wang, S., Chen, Q., 2019. Potential of Thirteen Urban Greening Plants to Capture
 561 Particulate Matter on Leaf Surfaces across Three Levels of Ambient Atmospheric Pollution.
 562 *Int. J. Environ. Res. Public Health* 16, 402. <https://doi.org/10.3390/ijerph16030402>
 563 Long, C.M., Nascarella, M.A., Valberg, P.A., 2013. Carbon black vs. black carbon and other
 564 airborne materials containing elemental carbon: Physical and chemical distinctions. *Environ.*
 565 *Pollut.* 181, 271–286. <https://doi.org/10.1016/j.envpol.2013.06.009>
 566 Metcalfe, D.J., 2005. *Hedera helix* L. *J. Ecol.* 93, 632–648. [https://doi.org/doi:10.1111/j.1365-](https://doi.org/doi:10.1111/j.1365-2745.2005.01021.x)
 567 [2745.2005.01021.x](https://doi.org/doi:10.1111/j.1365-2745.2005.01021.x)
 568 Mitsubishi Chemical, n.d. Application Examples of Carbon Black. URL
 569 <http://www.carbonblack.jp/en/cb/youto.html> (accessed 10.26.19).
 570 Morawska, L., Xiu, M., He, C., Buonanno, G., McGarry, P., Maumy, B., Stabile, L., Thai, P.K.,
 571 2019. Particle Emissions from Laser Printers: Have They Decreased? *Environ. Sci. Technol.*
 572 *Lett.* 6, 300–305. <https://doi.org/10.1021/acs.estlett.9b00176>
 573 Muhammad, S., Wuyts, K., Samson, R., 2019. Atmospheric net particle accumulation on 96 plant
 574 species with contrasting morphological and anatomical leaf characteristics in a common
 575 garden experiment. *Atmos. Environ.* 202, 328–344.
 576 <https://doi.org/10.1016/j.atmosenv.2019.01.015>
 577 Myers, I., Maynard, R.L., 2005. Polluted air - Outdoors and indoors. *Occup. Med. (Chic. Ill).* 55,

578 432–438. <https://doi.org/10.1093/occmed/kqi137>

579 Petzold, A., Ogren, J.A., Fiebig, M., Laj, P., Li, S.-M., Baltensperger, U., Holzer-Popp, T., Kinne,
580 S., Pappalardo, G., Sugimoto, N., Wehrli, C., Wiedensohler, A., Zhang, X.-Y., 2013.
581 Recommendations for reporting “black carbon” measurements. *Atmos. Chem. Phys.* 13,
582 8365–8379. <https://doi.org/10.5194/acp-13-8365-2013>

583 Petzold, A., Schloesser, H., Sheridan, P.J., Arnott, W.P., Ogren, J.A., Virkkula, A., 2005.
584 Evaluation of Multiangle Absorption Photometry for Measuring Aerosol Light Absorption.
585 *Aerosol Sci. Technol.* 39, 40–51. <https://doi.org/10.1080/027868290901945>

586 Popek, R., Gawrońska, H., Wrochna, M., Gawroński, S.W., Sæbø, A., 2013. Particulate Matter on
587 Foliage of 13 Woody Species: Deposition on Surfaces and Phytostabilisation in Waxes - a 3-
588 Year Study. *Int. J. Phytoremediation* 15, 245–256.
589 <https://doi.org/10.1080/15226514.2012.694498>

590 Pugh, T.A.M., MacKenzie, A.R., Whyatt, J.D., Hewitt, C.N., 2012. Effectiveness of green
591 infrastructure for improvement of air quality in urban street canyons. *Environ. Sci. Technol.*
592 46, 7692–7699. <https://doi.org/10.1021/es300826w>

593 Robertson, J., 2002. Diamond-like amorphous carbon, *Materials Science and Engineering: R: Reports*. Elsevier. [https://doi.org/10.1016/S0927-796X\(02\)00005-0](https://doi.org/10.1016/S0927-796X(02)00005-0)

594

595 Ruprecht, A.A., De Marco, C., Saffari, A., Pozzi, P., Mazza, R., Veronese, C., Angellotti, G.,
596 Munarini, E., Ogliari, A.C., Westerdahl, D., Hasheminassab, S., Shafer, M.M., Schauer, J.J.,
597 Repace, J., Sioutas, C., Boffi, R., 2017. Environmental pollution and emission factors of
598 electronic cigarettes, heat-not-burn tobacco products, and conventional cigarettes. *Aerosol*
599 *Sci. Technol.* 51, 674–684. <https://doi.org/10.1080/02786826.2017.1300231>

600 Sæbø, A., Popek, R., Nawrot, B., Hanslin, H.M., Gawronska, H., Gawronski, S.W., 2012. Plant

species differences in particulate matter accumulation on leaf surfaces. *Sci. Total Environ.* 427–428, 347–354. <https://doi.org/10.1016/j.scitotenv.2012.03.084>

Saenen, N.D., Bové, H., Steuwe, C., Roeffaers, M.B.J., Provost, E.B., Lefebvre, W., Vanpoucke, C., Ameloot, M., Nawrot, T.S., 2017. Children’s urinary environmental carbon load: A novel marker reflecting residential ambient air pollution exposure? *Am. J. Respir. Crit. Care Med.* 196, 873–881. <https://doi.org/10.1164/rccm.201704-0797OC>

Schwarz, J.P., Spackman, J.R., Gao, R.S., Perring, A.E., Cross, E., Onasch, T.B., Ahern, A., Wrobel, W., Davidovits, P., Olfert, J., Dubey, M.K., Mazzoleni, C., Fahey, D.W., 2010. The Detection Efficiency of the Single Particle Soot Photometer. *Aerosol Sci. Technol.* 44, 612–628. <https://doi.org/10.1080/02786826.2010.481298>

Sharma, S., Leaitch, W.R., Huang, L., Veber, D., Kolonjari, F., Zhang, W., Hanna, S.J., Bertram, A.K., Ogren, J.A., 2017. An evaluation of three methods for measuring black carbon in Alert, Canada. *Atmos. Chem. Phys* 17, 15225–15243. <https://doi.org/10.5194/acp-17-15225-2017>

Snyder, E.G., Watkins, T.H., Solomon, P.A., Thoma, E.D., Williams, R.W., Hagler, G.S.W., Shelow, D., Hindin, D.A., Kilaru, V.J., Preuss, P.W., 2013. The Changing Paradigm of Air Pollution Monitoring. *Environ. Sci. Technol.* 47, 11369–11377. <https://doi.org/10.1021/es4022602>

Stabile, L., Jayaratne, E.R., Buonanno, G., Morawska, L., 2014. Charged particles and cluster ions produced during cooking activities. *Sci. Total Environ.* 497–498, 516–526. <https://doi.org/10.1016/j.scitotenv.2014.08.011>

Sternberg, T., Viles, H., Cathersides, A., Edwards, M., 2010. Dust particulate absorption by ivy (*Hedera helix* L) on historic walls in urban environments. *Sci. Total Environ.* 409, 162–168. <https://doi.org/10.1016/j.scitotenv.2010.09.022>

- Tang, T., Hurraß, J., Gminski, R., Mersch-Sundermann, V., 2012. Fine and ultrafine particles emitted from laser printers as indoor air contaminants in German offices. *Environ. Sci. Pollut. Res.* 19, 3840–3849. <https://doi.org/10.1007/s11356-011-0647-5>
- United States Environmental Protection Agency, 2019. Indoor Particulate Matter | Indoor Air Quality (IAQ) | US EPA. US EPA. URL <https://www.epa.gov/indoor-air-quality-iaq/indoor-particulate-matter>
- Watson, J.G., Chow, J.C., Chen, L.-W.A., 2005. Summary of Organic and Elemental Carbon/Black Carbon Analysis Methods and Intercomparisons. *Aerosol Air Qual. Res.* 5, 65–102. <https://doi.org/10.4209/aaqr.2005.06.0006>
- Weingartner, E., Saathoff, H., Schnaiter, M., Streit, N., Bitnar, B., Baltensperger, U., 2003. Absorption of light by soot particles: Determination of the absorption coefficient by means of aethalometers. *J. Aerosol Sci.* 34, 1445–1463. [https://doi.org/10.1016/S0021-8502\(03\)00359-8](https://doi.org/10.1016/S0021-8502(03)00359-8)
- Wojdyr, M., 2010. *Fityk* : a general-purpose peak fitting program. *J. Appl. Crystallogr.* 43, 1126–1128. <https://doi.org/10.1107/S0021889810030499>